Full utilization of semi-Dirac cones in photonics

Utku G. Yasa,[1,*] Mirbek Turduev,[2] Ibrahim H. Giden,[1] and Hamza Kurt[1]
[1]*Department of Electrical and Electronics Engineering, TOBB University of Economics and Technology, 06560 Ankara, Turkey*
[2]*Department of Electrical and Electronics Engineering, TED University, 06420 Ankara, Turkey*

(Received 10 January 2018; revised manuscript received 4 May 2018; published 16 May 2018)

In this study, realization and applications of anisotropic zero-refractive-index materials are proposed by exposing the unit cells of photonic crystals that exhibit Dirac-like cone dispersion to rotational symmetry reduction. Accidental degeneracy of two Bloch modes in the Brillouin zone center of two-dimensional C_2-symmetric photonic crystals gives rise to the semi-Dirac cone dispersion. The proposed C_2-symmetric photonic crystals behave as epsilon-and-mu-near-zero materials ($\varepsilon^{\text{eff}} \approx 0$, $\mu^{\text{eff}} \approx 0$) along one propagation direction, but behave as epsilon-near-zero material ($\varepsilon^{\text{eff}} \approx 0$, $\mu^{\text{eff}} \neq 0$) for the perpendicular direction at semi-Dirac frequency. By extracting the effective medium parameters of the proposed C_4- and C_2-symmetric periodic media that exhibit Dirac-like and semi-Dirac cone dispersions, intrinsic differences between isotropic and anisotropic materials are investigated. Furthermore, advantages of utilizing semi-Dirac cone materials instead of Dirac-like cone materials in photonic applications are demonstrated in both frequency and time domains. By using anisotropic transmission behavior of the semi-Dirac materials, photonic application concepts such as beam deflectors, beam splitters, and light focusing are proposed. Furthermore, to the best of our knowledge, semi-Dirac cone dispersion is also experimentally demonstrated for the first time by including negative, zero, and positive refraction states of the given material.

DOI: 10.1103/PhysRevB.97.195131

I. INTRODUCTION

Photonic crystals (PCs) are periodically (or quasiperiodically) index-modulated structures that exhibit extraordinary light manipulation characteristics with the help of strong light-matter interaction inside them [1,2]. The ongoing demand for the efficient control of light makes these artificially generated structures an important solution in the fields of nanoscale optics and photonics. Ever since the first introduction of them to the literature, numerous wave transport and dispersion phenomena of PCs have been discovered, such as photonic band gaps [3], negative refraction [4], self-collimation [5], and superprisms [6]. The photonic Dirac cone dispersion is one of these phenomena and is formed by a linear conical singularity at the Brillouin zone corners of hexagonal-lattice periodic structures [7,8]. This linear conical singularity is an optical analog to the case in electronic solid-state systems like graphene, since it shows important electronic transport characteristics like the quantum Hall effect [9] and Zitterbewegung [10]. Recently, starting with the study of Huang *et al.* [11], the scope of photonic Dirac cones has been extended by demonstrating a new type of conical dispersion relation, i.e., Dirac-like cone dispersion [11–18]. Dirac-like cone dispersion shows up around the Brillouin zone center of PCs that consist of unit cells including dielectric rods having specific structural parameters. At a Dirac-like point, the periodic medium behaves as an isotropic epsilon-and-mu-near-zero (EMNZ) medium. The EMNZ materials have both their effective medium parameters converge to zero ($\varepsilon^{\text{eff}} \approx \mu^{\text{eff}} \approx 0$) and using this peculiar behavior one can realize zero-refractive-index PC-based novel photonic applications such as unidirectional transmission [19], beam focusing [20], and obstacle cloaking [11]. Prior to the mentioned studies about PCs having Dirac-like cone dispersion, previous researches [21–27] have achieved and investigated the zero-refractive-index phenomenon by different concepts such as materials that contain metallic components. However, since the effective medium parameters of these materials do not approach zero simultaneously ($\varepsilon^{\text{eff}} \approx 0$, $\mu^{\text{eff}} \neq 0$ or $\varepsilon^{\text{eff}} \neq 0$, $\mu^{\text{eff}} \approx 0$), these structures have high intrinsic optical losses or impedance mismatch. Also, they can be grouped under two titles according to the values of their optical parameters: epsilon-near-zero (ENZ $\rightarrow$ $\varepsilon^{\text{eff}} \approx 0$, $\mu^{\text{eff}} \neq 0$) and mu-near-zero (MNZ $\rightarrow$ $\varepsilon^{\text{eff}} \neq 0$, $\mu^{\text{eff}} \approx 0$) materials.

The enthusiasm to design artificial media that exhibit zero refractive index lies behind the unusual interaction of electromagnetic waves with these materials, whether they are single-zero (ENZ or MNZ) or double-zero (EMNZ) material. According to Snell's law, one physical indication of zero refractive index is that the refraction angle of waves exiting from these structures is equal to 0°. This allows waves to leave zero-refractive-index material along the direction which is perpendicular to the air-material interface. In addition, since Snell's law must be met, high reflection occurs at the material's surface if the angle of incidence of waves is other than 0°. The convergence of the refractive index to zero provides for the wavelength of the propagating electromagnetic wave inside these materials to be extremely large. Thus, extremely large wavelength ensures that waves propagate without reflection losses at waveguide bends filled with zero-refractive-index materials. In other words, waves can be tunneled through

*Corresponding author: gorkemyasa@etu.edu.tr

very narrow and sharp channels in an efficient manner [27]. Moreover, the phase distribution inside zero-refractive-index materials is uniform due to large wavelength. Therefore, these structures are also able to engineer the shape of wave fronts thanks to the uniform profile of phase distribution [23]. In other words, one can obtain the desired radiation pattern by truncating the air-material interface in a required manner.

The Dirac-like cone dispersion existing at $\mathbf{k} = 0$ can be considered a crucial alternative to obtain impedance-matched zero-refractive-index materials without utilizing lossy inclusions. Furthermore, PCs exhibiting Dirac-like cone dispersion behave as an isotropic material at Dirac-like points since both effective medium parameters approach zero for every propagation direction. The electromagnetic wave propagation inside an EMNZ material continues along all directions, so the utilization of confining metallic materials that limit light propagation along undesirable directions should be considered. In addition, it is known that the Dirac-like cone dispersion is formed by the specific structural parameters of the PC unit cells and there is only one Dirac-like point frequency for the unit cell parameters chosen. This structural uniqueness is undesirable for photonic applications that may require the zero-refractive-index property at different frequencies or different PC configurations. The above-discussed limitations may complicate configurability of the Dirac-like cone-dispersion-based photonic devices in fabrication and utilization processes.

In this paper, as an alternative solution to the above-stated limitations in PCs having Dirac-like cone dispersion, we both numerically and experimentally investigate the semi-Dirac cone dispersion phenomenon in PCs with reduced rotational symmetry. In spite of isotropic artificial media exhibiting Dirac-like cone dispersion, periodic structures having semi-Dirac cone dispersion possess anisotropic zero-refractive-index behavior [28,29]. We focus on the advantages of symmetry-reduced (or low-symmetric) PCs having semi-Dirac cone dispersion. Also, possible photonic applications employing the semi-Dirac cone phenomenon are also presented. In contrast with Dirac-like cone materials, the designed semi-Dirac structures show the low-loss EMNZ characteristic for one propagation direction, but an impedance-mismatched ENZ behavior for the perpendicular direction. Thus, the designed photonic structures, which are based on semi-Dirac dispersion, transmit most of the incident power along one propagation direction without the need for confining materials.

Even though the works in Refs. [28,29] introduced the semi-Dirac cone dispersion phenomenon to the photonic literature, there are additional important points that still need to be investigated. The PC structure proposed in Ref. [28] is limited to one type of unit cell configuration (elliptical dielectric rods) to form semi-Dirac cone dispersion. Also, only a specific size of the elliptical dielectric rods is considered in that study. On the other hand, in the present work, we extend the appearance of semi-Dirac cone dispersion by analyzing different lattice types (rectangular and square) and unit cell configurations (circular and rectangular dielectric rods). Here, we propose a rectangular lattice of perfectly circular dielectric rods, which may provide a feasible implementation of the semi-Dirac cone phenomenon. In addition, we also demonstrate the structural configurability of semi-Dirac frequency by controlling the geometrical parameters of dielectric rods. This structural configurability can be useful in potential applications in the fields of optics and photonics where the fabrication and design restrictions may take place. Also, the presented study provides the possible utilization of semi-Dirac cone dispersion in photonic applications. Finally, to the best of our knowledge, this is the first time that semi-Dirac cone dispersion is verified experimentally in the microwave domain.

II. SPECTRAL AND TIME DOMAIN ANALYSES

The rotational symmetry reduction in PCs stands for a degradation in the rotational symmetry order of the PC unit cells by changing the aspect ratios of the dielectric rods or by including additional dielectric elements [30–32]. As already known, geometric properties of the unit cells have a significant role in determining the optical response of periodic structures in the spectral domain. The rotational symmetry is one of these determinant characteristics that influence the interaction of PCs with electromagnetic waves [33,34]. The PC unit cells can be grouped under different orders of rotational symmetry ($C_1, C_2, C_3, C_4, \ldots C_n$) according to their geometrical configurations and lattice types. For instance, square-shaped dielectric rods that form a square-lattice PC are grouped within the C_4 rotational symmetry group. The reason is that the square-shaped figures present the same appearance after they are rotated by 90° around their center point. Here, the order number "4" comes from the ratio between rotation (90°) for the square case and full rotation (360°).

Figure 1(a) represents an $(a \times a)$-sized C_4-symmetric unit cell having square dielectric rods, which form a two-dimensional square-lattice PC that exhibits Dirac-like cone dispersion. The material composing the dielectric rods was considered as InP (indium phosphide) for the applications in optical telecom wavelengths. Hence, the permittivity of dielectric rods was fixed to be $\varepsilon = 10.04$ and the structural parameters are $b_1 = 0.378a$ and $c_1 = 0.378a$, where "a" is the lattice constant of the periodic medium. Here, given PC unit cells can be gathered under the C_4 rotational symmetry group, since the required rotation degree to obtain the same appearance is 90°. In order to calculate the spectral properties of the PC, frequency domain analyses are performed by exploiting the plane wave expansion method [35]. Figure 1(b) represents the transverse-magnetic (TM) polarization photonic band structure of the square-lattice PC, where the nonzero electric and magnetic field components are defined as E_z, H_x, and H_y, respectively. Here, the electric field component (E_z) is along the axis of the dielectric rods (z axis), and magnetic field components (H_x, H_y) are transverse to the axis of dielectric rods. In other words, we adapt the notion of polarization classification used in two-dimensional PCs. The corresponding directions of the x, y, and z axes are given as an inset plot in Fig. 1(a).

As can be seen from Fig. 1(b), in the Brillouin zone center, the second, third, and fourth dispersion curves accidentally intersect at a triply degenerate point ($a/\lambda = 0.566$), which is marked as "A1." In other words, point A1 is created by the accidental degeneracy of three Bloch states at the Γ point. Here, the term "accidental" means that the modes for the triply degenerate Bloch states are adjusted to intersect at the Γ point by tuning the structural parameters of dielectric rods. This

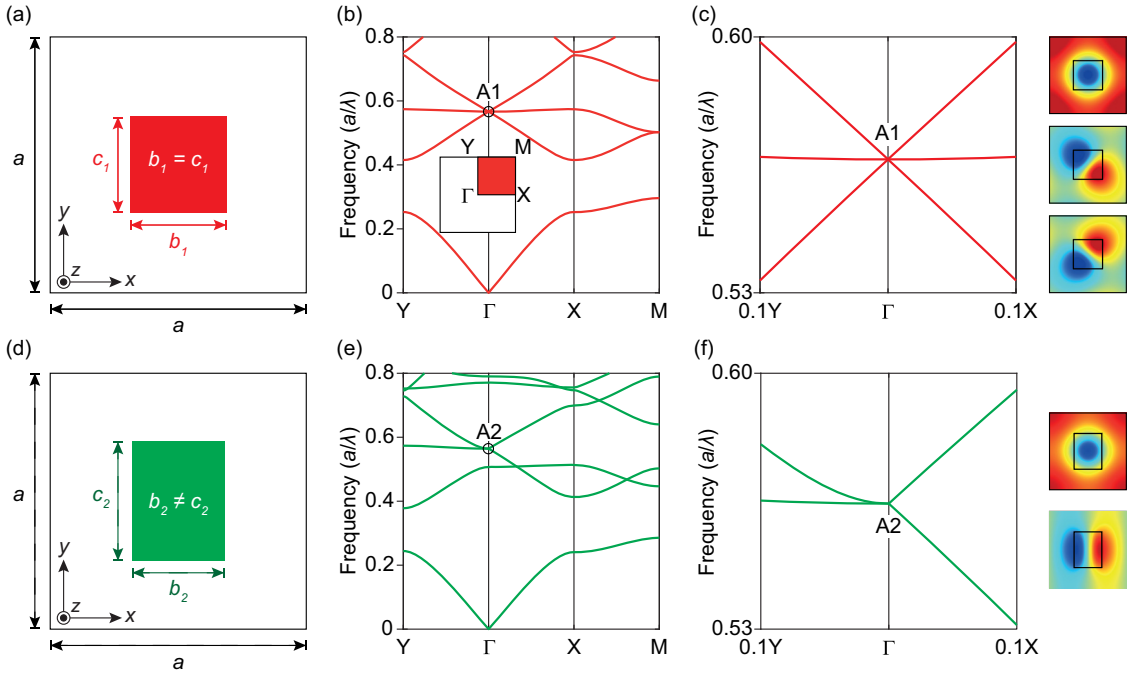

FIG. 1. The unit cell configurations and the photonic band structures of two-dimensional (2D) square-lattice PCs exhibiting Dirac-like and semi-Dirac cone dispersions. (a) 2D representation of a C_4-symmetric unit cell that consists of a square dielectric rod with structural parameters $b_1 = 0.378a$, $c_1 = 0.378a$, and permittivity $\varepsilon = 10.04$. (b) TM polarization band structure of the PCs formed by square dielectric rods. In the center of the Brillouin zone, three bands intersect at the Dirac-like point frequency $a/\lambda = 0.566$, which is marked as A1. The Brillouin zone is given as an inset. (c) A zoomed view of the Dirac-like cone dispersion comprises of two flat bands and four linear bands. (d) 2D representation of a C_2-symmetric unit cell that consists of a rectangular dielectric rod with structural parameters $b_2 = 0.360a$, $c_2 = 0.465a$, and permittivity $\varepsilon = 10.04$. (e) TM polarization band structure of the PCs formed by rectangular dielectric rods. In the center of the Brillouin zone, two bands intersect at the semi-Dirac point frequency $a/\lambda = 0.564$, which is marked as A2. (f) A zoomed view of the semi-Dirac cone dispersion that comprises a flat band, a quadratic band, and two linear bands.

intersection point is referred as the Dirac-like point and the dispersion relation around point A1 is named the Dirac-like cone dispersion. At Dirac-like frequency, the PC behaves as an isotropic EMNZ material where the dispersion relation in the vicinity of the Dirac-like point is linear and eigenstates of the triply degenerate point consist of one monopolar and two dipolar modes. Figure 1(c) is prepared to analyze band characteristics near the Dirac-like point and the electric field eigenstates at the triply degenerate point. The given band structure in Fig. 1(c) is formed by four linear bands and two flat bands near the Dirac-like point. Moreover, electric field eigenstates at point A1 consist of one monopolar mode along with two dipolar modes as can be seen from the given insets. These calculations confirm that the given dispersion relation can be treated as a Dirac-like cone dispersion and the given C_4-symmetric PC behaves as an EMNZ material at the Dirac-like point.

As mentioned before, all-dielectric PC structures with accidentally degenerated Bloch modes having Dirac-like conical dispersion behave as an isotropic EMNZ medium. On the other hand, in some cases, certain photonic designs may require the anisotropic nature of the PC dispersion relations to efficiently route, transport, and tailor the light beams. Inducing optical anisotropy to an isotropic material can be achieved by infiltration of the host medium by anisotropic materials or by the tuning structural configuration (unit cell's shape, symmetry, or type). Also, the optical properties of the former approaches can be dynamically configured by applying an external electric field [36–41]. The latter method is about tailoring the isofrequency contours of PCs by introducing a certain amount of reduction to PC unit cells' rotational symmetry [30,31,42]. In this study, we have considered the second approach, i.e., the rotational symmetry reduction, as a good solution to transform an isotropic EMNZ structure into anisotropic one. Figure 1(d) shows a two-dimensional PC unit cell representation composed of a C_2-symmetric rectangular dielectric rod having structural parameters that are equal to $b_2 = 0.360a$ and $c_2 = 0.465a$ with the permittivity of $\varepsilon = 10.04$. As can be deduced from the given schematic, the aspect ratio of the rectangular rods differs from unity due to the symmetry reduction in the unit cell elements. The photonic band structure of the C_2-symmetric PC is prepared in Fig. 1(e) to be able to observe the impact of introducing a rotational symmetry reduction. Differently from the Dirac-like cone case in Fig. 1(b), only two dispersion bands (third and fourth bands) accidentally intersect at a doubly degenerate point "A2," which is called a semi-Dirac point [see Fig. 1(f)]. At semi-Dirac frequency, the PC structure shows an anisotropic behavior, i.e., behaving as an EMNZ material along the ΓX propagation direction and as an ENZ medium for the ΓY direction. Similar to the Dirac-like cone case in Fig. 1(c), symmetry-reduced PCs exhibiting semi-Dirac cone dispersion must meet certain requirements to be related with zero-refractive-index behavior [28]. First, the photonic band structure near the semi-Dirac

frequency should involve a linear relation for one symmetry axis and a quadratic band along with a flat band for the other symmetry axis. Second, electric field eigenstates at $\mathbf{k} = 0$ must provide one monopolar mode and one dipolar mode. With the intent of examining whether the given C_2-symmetric PC meets these criteria or not, a zoomed version of the band structure near the semi-Dirac point is represented in Fig. 1(f) to check the dispersive requirements of the semi-Dirac cone. It can be deduced from the figure that the dispersion relation near point A2 is formed by a flat band along with a quadratic band for the ΓY propagation direction and two linear bands for the ΓX propagation direction. Moreover, eigenstates at the doubly degenerate point are composed of one monopolar mode and one dipolar mode. The performed calculations imply that the doubly degenerate dispersion relation of the C_2-symmetric PC structure can be considered semi-Dirac dispersion.

The finite-difference time-domain (FDTD) method [43] is performed to analyze time domain responses of the proposed PCs exhibiting Dirac-like and semi-Dirac cone dispersions. The given triangle-shaped PCs are excited by a source with a Gaussian spatial profile operating at Dirac-like and semi-Dirac frequencies [see the FDTD results shown in Figs. 2(a) and 2(b)]. Figure 2(a) demonstrates the electric field distribution inside the C_4-symmetric triangle-shaped PC structure exhibiting Dirac-like cone dispersion. The proposed medium is excited at the Dirac-like point $a/\lambda = 0.566$ and the triangle-shaped structure functions as a beam splitter at the Dirac-like point frequency. The corresponding FDTD result represents two typical characteristics of light-matter interaction in an EMNZ medium. First, the phase distribution inside the periodic medium has a uniform property since the phase velocity (or wavelength) inside the PC structure converges to infinity. Second, in parallel with Snell's law, wave fronts exiting from the triangular PC edges have a plane-wave characteristic, which mimics the shape of the air-PC interface as expected from an EMNZ medium. Since the PC structures exhibiting Dirac-like cone dispersion show an isotropic zero-refractive-index feature, incident beams exit along both ΓX and ΓY propagation directions with equal powers. However, this isotropic property may require additional components to confine the light along one propagation direction to realize some proper photonic applications.

Figure 2(b) shows the electric field distribution inside the C_2-symmetric PC structure exhibiting semi-Dirac cone dispersion and having the same triangle shape as the structure given in Fig. 2(a). The periodic medium is excited at the semi-Dirac point $a/\lambda = 0.564$. Asymmetric light coupling is clearly observed from Fig. 2(b); the anisotropic behavior of the semi-Dirac dispersion makes incident waves exit from the upper edge of the triangle, while the efficiency of light output at the bottom interface is dramatically low. At semi-Dirac frequency, calculated transmission efficiencies at the upper and bottom edges are $T_{\text{upper}} = 81.6457\%$ and $T_{\text{bottom}} = 0.0022\%$, respectively. This emerging phenomenon can be interpreted as the following: The proposed C_2-symmetric PC structure has an EMNZ characteristic along the ΓX propagation direction and an ENZ property for the ΓY case. As already known, the effective permittivity of ENZ materials converges to $\varepsilon^{\text{eff}} \approx 0$, whereas the effective permeability is $\mu^{\text{eff}} \neq 0$. Thus, since the effective permeability is not equal to zero, an optical impedance mismatch arises between the periodic medium and the surrounding air. The occurring optical impedance mismatch causes a reduction in the transmission efficiency for output beams propagating along the ΓY direction inside the PC and confines the light. On the other hand, along the ΓX direction, both effective permittivity and permeability are equal to zero, which makes the PC structure behave as an EMNZ medium toward the ΓX direction. The equality of effective constitutive parameters to zero makes the studied periodic structure optically impedance matched to air along the ΓX direction. These two conditions can be considered as the reason why the incident waves propagate through the ΓX direction but are confined along the ΓY direction. The indications of a zero-refractive-index feature can be observed in Fig. 2(b): First, the phase distribution inside the PC structure has a uniform manner like the Dirac-like cone case. Second, output beams from both triangle edges mimic the shape of the air-PC interface. It is important to note that, despite the impedance mismatch in the ΓY direction, the proposed PC structure still has a zero-refractive-index property at semi-Dirac frequency and the output wave fronts have a plane-wave characteristic even though the transmission value is still low. Such direction-dependent transmission behavior gives PCs with semi-Dirac cone dispersion an advantage over the periodic media exhibiting Dirac-like cone dispersion, in which case additional perfect-electric or perfect-magnetic conductors may be required to confine light along undesired propagation directions.

As is known, the wavelength of the propagating electromagnetic waves is very large (infinite in the ideal case) inside a zero-refractive-index material comparing to the wavelength in free space. This extraordinary effect enables electromagnetic waves to be spatially coherent at any point inside the structure, since the phase profile has a uniform distribution inside the medium. More specifically, the phase profile becomes uniformly distributed because the effective refractive index of the medium converges to zero and the corresponding wavelength approaches extremely larger values. It is also possible to maintain spatial phase coherence within the PC exhibiting semi-Dirac dispersion so that one can maintain directional emission even when multiple sources are embedded in the PC. Due to the zero-refractive-index phenomenon, emanating waves experience infinitely short optical path lengths ($\text{OPL} = (2\pi/\lambda)n^{\text{eff}}$) within the PC structure. Consequently, even though the point sources are located at finite distances from each other inside a zero-refractive-index material, there emerges a negligibly small optical path difference between the generated waves. In this case, it can be considered that the point sources are overlapped with each other regardless of their numbers and physical locations within the PC structure. Hence, one can deduce that the point sources superpose perfectly inside the PC structure and create an artificially new source. The superposed waves propagate as if they are generated from a single source where the wave fronts of exiting waves are parallel to the air-PC interface. As a result, the emerged coherence within the PC region due to the very small optical path length between the point sources provides the exiting waves with a constant phase in a plane perpendicular to the propagation direction. In other words, the emerged coherence within the PC structure also ensures the waves exiting from the periodic medium to be spatially coherent; i.e., the output

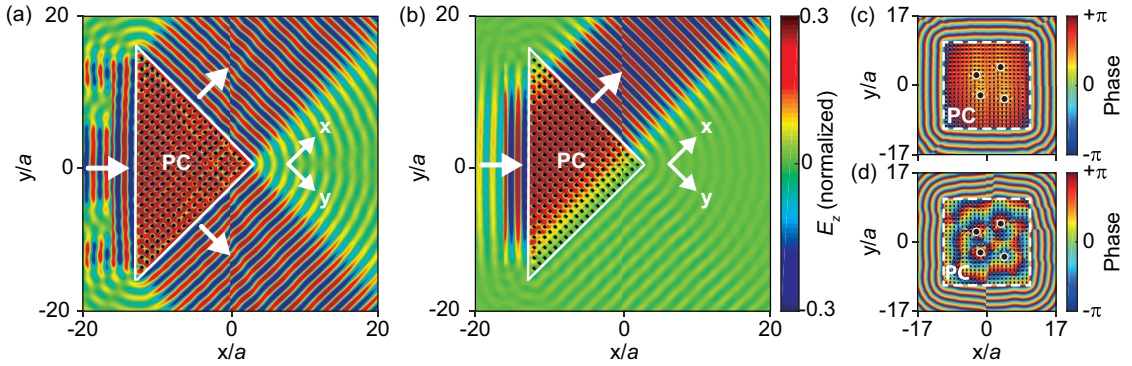

FIG. 2. Corresponding electric field and phase profiles showing light-matter interaction in periodic media with Dirac-like and semi-Dirac cone dispersions. (a) The electric field distribution inside the proposed C_4-symmetric PC having Dirac-like cone dispersion. The structure is excited by a Gaussian source operating at a Dirac-like point frequency $a/\lambda = 0.566$. (b) The electric field distribution inside the proposed C_2-symmetric PC having semi-Dirac cone dispersion. The structure is excited by a Gaussian source operating at a semi-Dirac frequency $a/\lambda = 0.564$. (c) The uniform phase profile inside the C_2-symmetric PC, which exhibits semi-Dirac cone dispersion. The given structure is excited by asymmetrically distributed four point sources operating near the semi-Dirac frequency $a/\lambda = 0.569$. (d) Nonuniform phase profile inside the same periodic medium. At this stage, the structure is excited by asymmetrically distributed four point sources operating at a normalized frequency $a/\lambda = 0.602$, in which the refractive index of the periodic medium is not $n^{\text{eff}} = 0$. In both figures, spatial locations of point sources are emphasized with black dots.

waves' phases in a plane perpendicular to the propagation direction is constant. The given square-lattice C_2-symmetric PC structure is excited by randomly distributed spatially and spectrally identical four point sources operating near the semi-Dirac frequency $a/\lambda = 0.569$, as shown in the phase distribution given in Fig. 2(c). Here, the black dots represent the locations of point sources inside the PC. As can be seen from the figure, the phase distribution within the structure is almost uniform, which results in a spatially coherent radiation pattern at the outside of the PC structure. In addition, due to the anisotropic behavior of semi-Dirac cone dispersion, the proposed PC structure enables wave propagation along the ΓX direction, whereas suppressing the exiting beam power along the ΓY direction [see Fig. 2(b)] leads to the formation of directional beams with enhanced power. In contrast, the directional feature and coherence effect of the propagating wave vanish when the PC structure is excited with identical four point sources operating at a frequency ($a/\lambda = 0.602$) away from the semi-Dirac point, as shown in Fig. 2(d).

By taking the advantage of an open discussion about the inherent spatial coherence phenomenon of the semi-Dirac cone materials, we want to further analyze that characteristic by making a possible connection with the well-known van Cittert–Zernike (VCZ) coherency theorem. The VCZ theorem is a coherence theory in classical optics and states that the emanating wave fronts from a spatially incoherent source exhibit a spatial coherence if one observes at a long distance under certain conditions [44]. For instance, if we consider the wave fronts generated by two spatially incoherent sources, one can see a spatially incoherent radiation pattern at a distance close to the sources. On the other hand, according to the VCZ theorem, if the observation is performed at longer distances from the sources, one can see that both sources will contribute almost equally to the wave fronts, which makes them spatially coherent. In our case, we have observed that, due to the extremely large wavelength inside the PC structure, spatial coherence can be obtained in an infinitely short distance using the PC structure given in Fig. 2(c). Therefore, in light of the above discussion, we can establish a possible analogy between the VCZ theorem and the semi-Dirac cone dispersion in terms of the generation of spatially coherent waves. In the case of the VCZ theorem the incoherent waves are transformed into spatially coherent ones at long distances. Introducing a zero-refractive-index material enables this transformation at infinitely short distances because of the extremely large wavelength and uniform phase profile within the structure. Here, we only propose a possible connection between two different phenomena. Thus, to make an extensive analysis of this connection, additional analytical and numerical investigations are required. For this reason, the detailed spatial coherence analyses can be further considered in future perspectives of this study.

Until now, isotropic and anisotropic zero-refractive-index features of given PCs have been demonstrated via electric field amplitude and phase profiles inside and outside of the structure. Nevertheless, the calculation of frequency-dependent effective medium parameters is also required to map proposed periodic structures to zero refractive index. In general, effective medium approaches are valid under the long-wavelength limit, i.e., in the low-frequency regime, where the wavelength is much larger than the periodicity of optical scatterers. Furthermore, concerned normalized frequency values in this study are comparatively not low enough to perform proper effective medium approaches. On the other hand, since Dirac-like and semi-Dirac points lie around the center of the Brillouin zone, an effective medium approach can still be applied [11]. Hence, to obtain the effective medium parameters, we have exploited the boundary effective medium concept, which was actually developed for elastic waves [45] and then implemented for PCs [28]. First, constitutive relations in Eq. (1) are considered to calculate effective medium parameters [28]:

$$\bar{D}_z = e^{\text{eff}}\bar{E}_z, \begin{bmatrix}\bar{B}_x \\ \bar{B}_y\end{bmatrix} = \begin{bmatrix}\mu_x^{\text{eff}} & 0 \\ 0 & \mu_y^{\text{eff}}\end{bmatrix}\begin{bmatrix}\bar{H}_x \\ \bar{H}_y\end{bmatrix}. \quad (1)$$

In Eq. (1), the average field values are calculated by eigenstate values at the unit cell boundaries. In the process of effective parameter extraction, the average field description is altered in accordance with the wave vector **k**. For example, for a PC structure, which is excited along the ΓX propagation direction, average electric and magnetic fields are given as

$$\bar{E}_z = \frac{\int_{-0.5a}^{0.5a} E_z(x=-0.5a)dy}{2a} + \frac{\int_{-0.5a}^{0.5a} E_z(x=0.5a)dy}{2a}, \tag{2}$$

$$\bar{H}_y = \frac{\int_{-0.5a}^{0.5a} H_y(x=-0.5a)dy}{2a} + \frac{\int_{-0.5a}^{0.5a} H_y(x=0.5a)dy}{2a}. \tag{3}$$

Furthermore, the average electric and magnetic field densities are

$$\bar{D}_z = \frac{\int_{-0.5a}^{0.5a} H_y(x=0.5a)dy}{-j\omega a^2} - \frac{\int_{-0.5a}^{0.5a} H_y(x=-0.5a)dy}{-j\omega a^2}, \tag{4}$$

$$\bar{B}_y = \frac{\int_{-0.5a}^{0.5a} E_z(x=0.5a)dy}{j\omega a^2} - \frac{\int_{-0.5a}^{0.5a} E_z(x=-0.5a)dy}{j\omega a^2}. \tag{5}$$

Here, the effective medium approach is performed by applying field averaging on the boundaries of eigenfields corresponding to the relevant wave vector (**k**). As mentioned before, the proposed periodic medium exhibiting semi-Dirac cone dispersion shows EMNZ and ENZ properties for the wave vectors lying along the the ΓX and ΓY symmetry axes. Thus, in this study, during the calculation of effective medium parameters, we considered two sets of wave vectors where $k_x = 0$, $k_y \neq 0$ for ΓX and $k_x \neq 0$, $k_y = 0$ for ΓY symmetry axes. Figures 3(a) and 3(b) show evaluated effective medium parameters for PCs exhibiting Dirac-like and semi-Dirac cone dispersions presented in Fig. 1, respectively. In Fig. 3(a), frequency-dependent optical parameters of C_4-symmetric PC structure are calculated along both ΓX and ΓY propagation directions. Here, since the considered medium has an isotropic dispersion, the calculated effective medium parameters along the ΓX direction are also the same for the ΓY case. Thus, the corresponding effective permittivity and permeability values along both directions overlap. As can be seen from Fig. 3(a), $\varepsilon_{x,y}^{\text{eff}}$ and $\mu_{x,y}^{\text{eff}}$ curves intersect at the Dirac-like point frequency $a/\lambda = 0.566$ and, in accordance with the previous comments, their effective values are $\varepsilon_{x,y}^{\text{eff}} \approx \mu_{x,y}^{\text{eff}} \approx 0$, which indicates that the proposed medium operates as an EMNZ medium along both ΓX and ΓY symmetry axes at the Dirac-like point. In addition to the zero-refractive-index feature, due to the continuous relation of effective medium parameters in the operating frequency range, the proposed structure behaves as a positive index material ($\varepsilon_{x,y}^{\text{eff}} > 0$ and $\mu_{x,y}^{\text{eff}} > 0$) above the Dirac-like frequency and has a negative refractive index ($\varepsilon_{x,y}^{\text{eff}} < 0$ and $\mu_{x,y}^{\text{eff}} < 0$) below the Dirac frequency. To compare the effective medium parameters of Dirac-like and semi-Dirac cone dispersions, similar calculations are performed for C_2-symmetric periodic medium [see Fig. 3(b)]. Since the C_2-symmetric unit cell exhibits an anisotropic dispersive behavior [see Fig. 1(e)], effective medium parameters along the ΓX and ΓY directions are expected to be different compared to the Dirac-like cone case. As can be seen in Fig. 3(b), the variation trend of effective permittivity ($\varepsilon_x^{\text{eff}}$) and permeability ($\mu_y^{\text{eff}}$) along the ΓX propagation direction is similar to the Dirac-like cone case. On the other hand, because of the anisotropic feature of C_2 symmetry, constitutive relations ($\varepsilon_y^{\text{eff}}$, μ_x^{eff}) along the ΓY direction exhibit different characteristics. Differently from the case of Dirac-like cone dispersion, here $\varepsilon_y^{\text{eff}}$ and μ_x^{eff} values do not intersect each other at the semi-Dirac frequency $a/\lambda = 0.564$. Moreover, although the effective permittivity crosses through $\varepsilon_y^{\text{eff}} \approx 0$, the effective permeability μ_x^{eff} never approaches zero ($\mu_x^{\text{eff}} \neq 0$). Therefore, this phenomenon gives rise to an ENZ material along the ΓY direction since the effective medium parameters are $\varepsilon_y^{\text{eff}} \approx 0$ and $\mu_x^{\text{eff}} \neq 0$ at the semi-Dirac frequency. As mentioned earlier, since the structure's effective permeability at the semi-Dirac frequency is $\mu_x^{\text{eff}} \neq 0$, the optical impedance $Z = \sqrt{\mu/\varepsilon}$ does not match with air and the corresponding transmission efficiency in the ΓY direction decreases. Here, it should be noted that between the normalized frequency interval of $a/\lambda = [0.507 - 0.564]$, data are unavailable for the ΓY direction due to the existence of a partial photonic band gap in that range.

As is already known, there is only a single triply degenerate point for the PCs consisting of dielectric rods having constant refractive index. The occurrence of the Dirac-like point for a certain value of the constructive parameters prevents triply degenerate Bloch states at the Γ point from being adjusted to desired frequencies. This single-frequency phenomenon may induce some restrictions in designing photonic applications that require zero-refractive-index materials. Furthermore, the structural parameters that reveal Dirac-like cone dispersion do not provide enough feasibility in the fabrication process. All these limitations push researchers to search alternative solutions of using the Dirac-like cone phenomenon in the design of photonic devices. One of the solutions that can be proposed is utilizing periodic media that exhibit the semi-Dirac dispersion relation. In order to investigate the structural configurability of the semi-Dirac dispersion phenomenon, structural parameters b_2 and C_2 of the C_2-symmetric rectangular rods [see Fig. 1(d)] are swept over a certain range. Next, they are taken as parameter sets to obtain different semi-Dirac frequencies, as shown in Fig. 3(c). The point represented by P_1 in the given figure represents the sizes of the C_4-symmetric square dielectric rods exhibiting Dirac-like cone dispersion. This point corresponds to the unit cell configuration given in Fig. 1(a). As we move away from this point, the unit cell structure is converted from C_4 to C_2 rotational symmetry and the aspect ratio of square dielectric rods differs from unity. It is important to note that the reduction in the rotational symmetry order of the dielectric rods leads to a conversion from the Dirac-like cone dispersion to the semi-Dirac cone dispersion. The emerging semi-Dirac points are obtained at different frequencies depending on the aspect ratios of the rectangular rods. For example, points P_2, P_3, and P_4 represent the semi-Dirac points corresponding to the different normalized frequencies and structural dimensions. Corresponding structural parameters of P_2, P_3, and P_4 semi-Dirac points

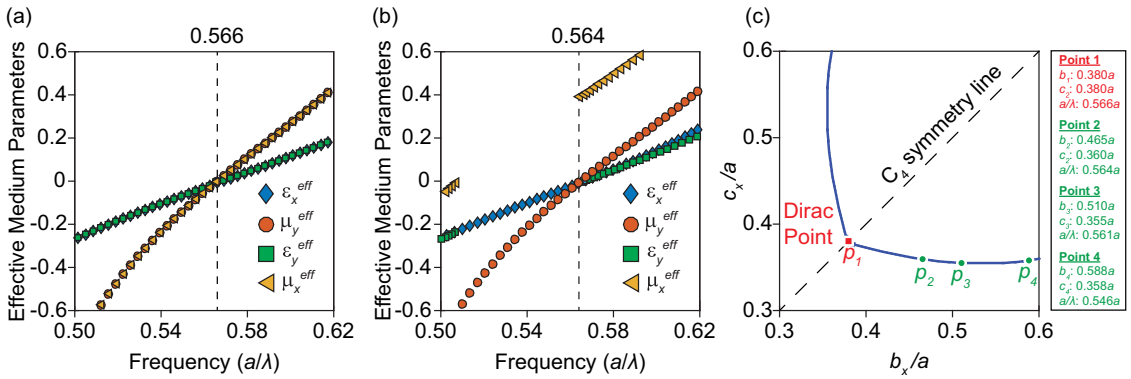

FIG. 3. Extracted effective medium parameters for Dirac-like and semi-Dirac cone materials and the semi-Dirac cone map. (a) Effective medium parameters for the given C_4-symmetric PC, which exhibits Dirac-like cone dispersion. All the effective values are equal to zero at the Dirac-like point $a/\lambda = 0.566$. (b) Effective medium parameters for the given C_2-symmetric PC, which exhibits semi-Dirac cone dispersion. $\varepsilon_x^{\text{eff}}$ and μ_y^{eff} represent the effective parameters along the ΓX propagation direction, whereas $\varepsilon_y^{\text{eff}}$ and μ_x^{eff} represent the ΓY case. (c) The structural parameter map with respect to b_x and c_x lengths of the dielectric rods. The red dot (p_1) represents the required width and length sizes for the C_4-symmetric dielectric rods to compose a PC structure having Dirac-like cone dispersion. Green dots (p_2, p_3, and p_4) show sample structural parameters for C_2-symmetric unit cell based PCs to realize semi-Dirac dispersion. The C_4-symmetry line is also represented with a dashed black line, which indicates the dielectric rods having b_x and c_x lengths equal.

are given as insets in Fig. 3(c). These remarks conclude that PCs having a semi-Dirac cone dispersion relation can be well adjusted to desired unit cell sizes and normalized frequencies.

As mentioned previously, the anisotropic behavior of semi-Dirac cone dispersion makes this dispersion relation more feasible for photonic applications. Compared to the Dirac-like cone case, which behaves as an isotropic medium, semi-Dirac materials exhibit high power flow along one direction (ΓX in our case) and confine the propagating light along the transverse direction (ΓY in our case). This means that light leakage along undesired directions is prohibited thanks to the direction-dependent role of the semi-Dirac effect and, moreover, there is not a necessity to use absorbing or reflector boundaries at the adjacent lateral interfaces. This particular spectral feature is an important solution when a PC structure is utilized in light manipulation applications that require directionality. In this regard, we have prepared several light manipulation applications by exploiting the anisotropic zero-refractive-index property of the studied C_2-symmetric PCs excited by a source operating at semi-Dirac frequency (see Fig. 4). The first light manipulation concept to be proposed is the deflection of light waves, which can be implemented by using the semi-Dirac cone dispersion relation, as shown in Fig. 4(a). In accordance with this purpose, rectangular dielectric rods are positioned in a triangular form both vertically and horizontally to form PC structures (triangular PCs are indicated by dashed white lines) and these triangle-shaped periodic media are cascaded to make a light deflection device. The proposed device provides a beam deflection of 90° with transmission efficiency $T = 70\%$ at semi-Dirac frequency. The second light-engineering concept is represented in Fig. 4(b), which is a PC beam splitter that consists of rectangular rods. The right edge of the given structure is truncated to form a half-octagonal shape. Since the exiting waves from an EMNZ medium mimic the air-EMNZ interface, the PC enables a splitting of incoming light into three output beams propagating along perpendicular to the output interfaces. Here, output transmission efficiencies at the exit interfaces are as follows: $T_1 = 26\%$, $T_2 = 37\%$, and $T_3 = 26\%$ along the upper, central, and bottom channels, respectively. As zero-refractive-index materials enable the engineering of wave fronts of outgoing waves, which mimic the air-material interface, the beam splitter phenomenon is not limited to the application given here. Power splitting of incoming radiation can be increased to the desired number of output channels by only truncating the edges of the PC structures. The last but not least application is the beam-focusing PC structure presented in Fig. 4(c). As is well known, the phase distribution inside a zero-refractive-index medium has a uniform profile due to the convergence of the wavelength to infinity. Moreover, in accordance with Snell's law, the propagation direction of electromagnetic waves exiting from these materials is always normal to the air-PC interface. Using this phenomenon, materials exhibiting Dirac-like cone dispersion can be exploited to design a focusing lens by modifying the output interface of the structure to form a concave shape [20]. However, as mentioned before, the isotropic feature of the Dirac-like cone dispersion requires a confining reflector material, since the light leakage along undesired directions weakens the focusing power. Lens designs based on the semi-Dirac dispersion phenomenon can be a good solution to this problem, since incoming radiation is confined along undesired directions. Figure 4(c) provides the focusing effect PC structure composed of rectangular rods. The concave lens focuses the incident light in a distance of $24.25a$ with a full width at half maximum of 0.661λ, where $\lambda = 1.773a$ and a is the lattice constant.

III. AN ALTERNATIVE REALIZATION VIA RECTANGULAR-LATTICE PHOTONIC CRYSTALS: NUMERICAL RESULTS WITH EXPERIMENTAL VERIFICATION

Until now, to reveal the semi-Dirac cone dispersion phenomenon, PCs with C_2-symmetric rectangular rods were considered. Even though the most up-to-date fabrication techniques provide fabrication of photonic structures in nanoscale, there are still some restrictions due to the structural and

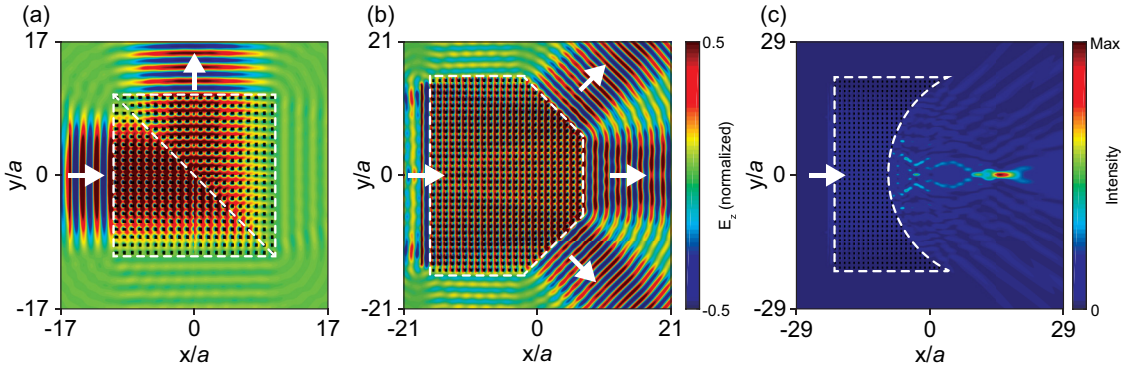

FIG. 4. Light beam manipulations by C_2-symmetric PCs operating at the semi-Dirac point. (a) Electric field distribution showing a beam-bending application, which exploits the self-confinement behavior of light inside C_2-symmetric PCs having semi-Dirac cone dispersion. (b) The electric field profile that demonstrates a beam splitter utilizing the wave-front shaping property of C_2-symmetric PCs with semi-Dirac cone dispersion. (c) The electric field intensity distribution showing a focusing lens composed of a semi-Dirac periodic medium. All of these structures are illuminated at the semi-Dirac frequency $a/\lambda = 0.564$.

geometrical complexity of PC structures. In this context, one can consider that the rectangular rods may encounter feasibility issues (due to possible fabrication imperfections) during the fabrication or realization process because of their sharp edges. Throughout the fabrication process, these sharp edges can be simply rounded due to the resolution limitations of the e-beam lithography (proximity effect of e-beam lithography) or chemical vapor deposition process [46] and it means that the produced PC unit cells' dielectric filling ratio has deviated from the numerically calculated one. Since dispersion properties are sensitive to the structural parameters of unit cells, possible fabrication imperfections may shift the semi-Dirac point or, worse, doubly degenerate Bloch states can simply vanish. In order to prevent the mentioned fabrication issues, we propose an alternative realization of semi-Dirac cone dispersion by utilizing perfectly circular dielectric rods aligned in a rectangular array. In Fig. 5(a), the two-dimensional (2D) representation of the rectangular-lattice periodic medium having circular dielectric rods with radii of $r = 0.262a$ and permittivity of $\varepsilon = 10.04$ is given. The unit cell parameters of the rectangular lattice are equal to $a_x = 1a$ and $a_y = 1.287a$. The corresponding TM polarization dispersion diagram for the given PC is depicted in Fig. 5(b). As can be observed from Fig. 5(b), two Bloch states (third and fourth dispersion bands) accidentally intersect at a doubly degenerate point in the Brillouin zone center at normalized frequency $a/\lambda = 0.486$ and generate a semi-Dirac point. We expect that, at semi-Dirac frequency, the given rectangular-lattice PC behaves as an anisotropic medium, i.e., an EMNZ medium along the ΓX propagation direction and and ENZ medium for the ΓY propagation direction. In order to prove this, effective medium parameters along both ΓX and ΓY propagation directions are calculated and presented in Fig. 5(c). The effective medium parameters have a similar trend compared to the square-lattice case. As can be seen from Fig. 5(c), all the effective parameters are equal to zero at the semi-Dirac frequency $a/\lambda = 0.486$ except μ_x^{eff}. As a consequence, the given results show that one can generate a semi-Dirac cone dispersion by utilizing not only a square array of rectangular rods but also a rectangular lattice of circular rods, which simplifies the fabrication process by avoiding the use of dielectric rods with sharp edges.

As mentioned before, the allure of the semi-Dirac cone dispersion is not only limited to the zero-refractive-index property; it also helps us realize negative-refractive-index and positive-refractive-index artificial materials. To experimentally verify all the effective refractive-index properties of PCs having the semi-Dirac dispersion relation, a rectangular-lattice PC structure composed of circular Al_2O_3 (alumina) rods with 99.8% purity was constructed [see Fig. 6(a)]. The rectangular unit cell representation and the photonic band structure of the alumina PC can also be seen in Fig. 6(a). Moreover, corresponding effective medium parameters of the designed PC structure composed of alumina rods are given in Fig. 6(b). Since we wanted to perform this experiment using the materials available at our disposal, we chose to utilize circular alumina rods aligned in a rectangular-lattice configuration. The permittivity of alumina rods is $\varepsilon = 9.8$ in the microwave regime and their radii and heights are $r = 3.175$ mm and $h = 152$ mm, respectively. During the design process of the PC structure, we intended to construct a periodic structure with the same filling ratio as the structures given in Figs. 1(d) and 5(a). Furthermore, the constructed PC structure was configured to form a semi-Dirac dispersion relation in the Brillouin zone center and the corresponding semi-Dirac frequency was calculated to be $f = 12.10$ GHz for the lattice constant of $a = 12.245$ mm. For the given rod radii and the lattice constant, the semi-Dirac cone dispersion occurs when the lattice sizes of the rectangular unit cells are equal to $a_x = 12.245$ mm and $a_y = 15.453$ mm. At semi-Dirac frequency, effective medium parameters are equal to $\varepsilon_x^{\text{eff}} = -0.005$ and $\mu_y^{\text{eff}} = -0.002$ along the ΓX symmetry axis while $\varepsilon_y^{\text{eff}} = -0.005$ and $\mu_x^{\text{eff}} = 0.312$ for the ΓY symmetry axis as shown in Fig. 6(b). The visual representation of the microwave experimental setup can be seen in Fig. 6(c). Microwaves were generated between the bandwidth of 6–18 GHz via an Agilent E5071C ENA vector network analyzer. The generated microwaves were injected into the periodic structure along the ΓX propagation direction with the aid of a horn antenna, which was aligned to the perpendicular edge (lying along the y direction) of the triangle-shaped PC structure. A monopole antenna was connected to the same network analyzer and measured the electric field distribution of the waves inside and outside of the triangle-shaped PC. The field measurements

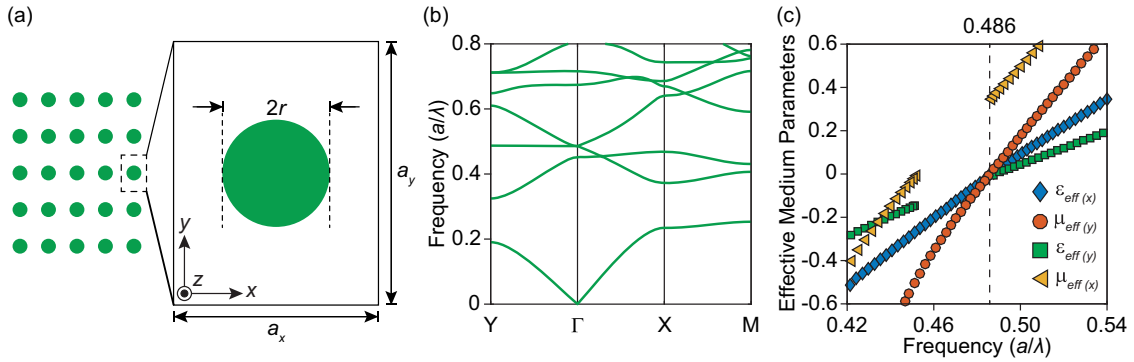

FIG. 5. An alternative realization of semi-Dirac dispersion by utilizing a rectangular lattice of circular rods. (a) 2D representation of a rectangular-lattice PC that consists of circular dielectric rods with radius $r = 0.262a$ and permittivity $\varepsilon = 10.04$. The size of the rectangular unit cell frame is equal to $a_x = 1a$ and $a_y = 1.287a$. (b) The TM polarization photonic band structure for the PC consists of a given unit cell. The semi-Dirac point can be observed in the Brillouin zone center at a normalized frequency $a/\lambda = 0.486$. (c) Effective medium parameters along both ΓX and ΓY propagation directions.

representing the electric field distribution inside of the PC were taken by sweeping the monopole antenna over the top of the dielectric rods. In addition, measurements representing the electric field profile along the hypotenuse and short edges of the structure were taken by scanning along the PC surface with the monopole antenna that was brought to the vertical midpoints of the dielectric rods. The electric distribution on the exit surfaces of the triangle-shaped PC was measured with a 2-mm step size.

Figures 7(a) and 7(b) show FDTD and experimental electric field results inside and outside of the PC structure given in Fig. 6(a). In the numerical solution case, the proposed structure was excited by a Gaussian source operating at a frequency ($f = 11.70$ GHz) below the semi-Dirac point. On the other hand, Fig. 7(b) represents the measured electric field profile at the same frequency. If one examines the results, it can be seen that both output field profiles show similar phase fluctuations inside the structures. Furthermore, since both effective medium parameters are negative [$\varepsilon^{\text{eff}} < 0$, $\mu^{\text{eff}} < 0$; see Fig. 6(b)] below the semi-Dirac point, the electromagnetic waves exiting from the PC edges are refracted negatively in both numerical and experimental results. Using the effective medium approach given in Fig. 6(b), at $f = 11.7$ GHz, the effective refractive index along the ΓX symmetry axis is determined as $n_x^{\text{eff}} = -0.166$. To validate the effective medium calculations, the refractive index is also calculated by measuring the exit angles of waves exiting from the hypotenuse. The measured effective refractive indices for both simulation and experimental results are $n_x^{\text{eff}} \approx -0.168$ (measured, simulation) and $n_x^{\text{eff}} \approx -0.168$ (measured, experiment), respectively. On the other hand, Figs. 7(c) and 7(d) represent the numerical and measured experimental results when the periodic medium is excited at the semi-Dirac frequency ($f = 12.10$ GHz). It is important to note that zero-refractive-index behavior, which is a consequence of the semi-Dirac dispersion relation, is readily apparent in both simulation and experimental results. The first indication is the uniform phase profile inside the structures, since the wavelength of electromagnetic waves inside the PCs converges to infinity. The latter indication is the plane-wave-like wave fronts of the beams exiting from PC edges, as they mimic the PC-air interface and make a refraction angle of $\theta_{\text{out}} = 0^\circ$ with the normal in accordance with Snell's law. Here, it is important to emphasize that the transmitted power along the y propagation direction is relatively lower than the power exiting from the hypotenuse

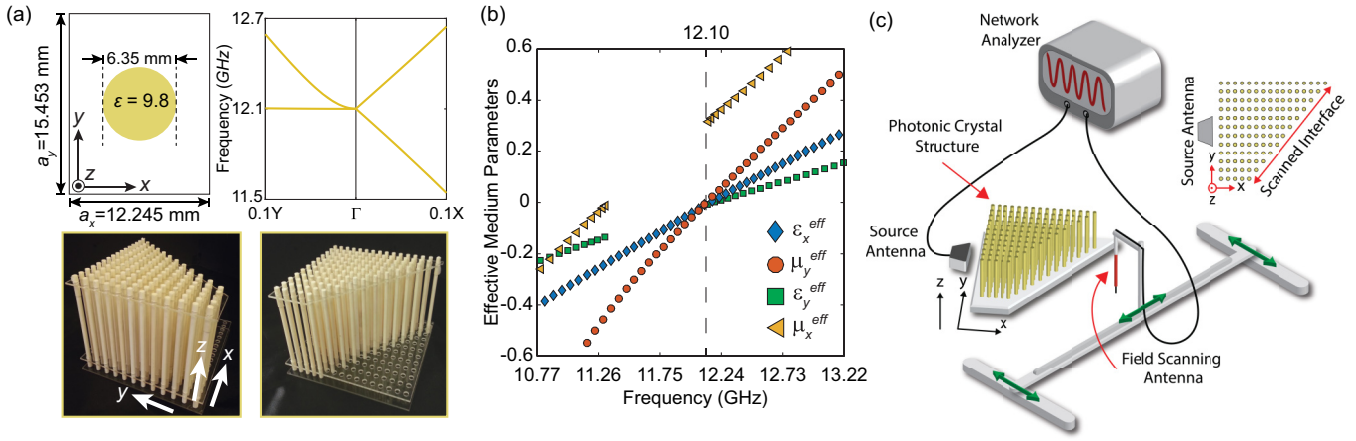

FIG. 6. The alumina PC and microwave experimental setup. (a) The constructed triangle-shaped rectangular-lattice alumina PC and corresponding unit cell representation with photonic band structure that exhibits semi-Dirac cone dispersion. (b) The calculated effective medium parameters of the proposed alumina PC. (c) Three-dimensional visualization of the experimental setup.

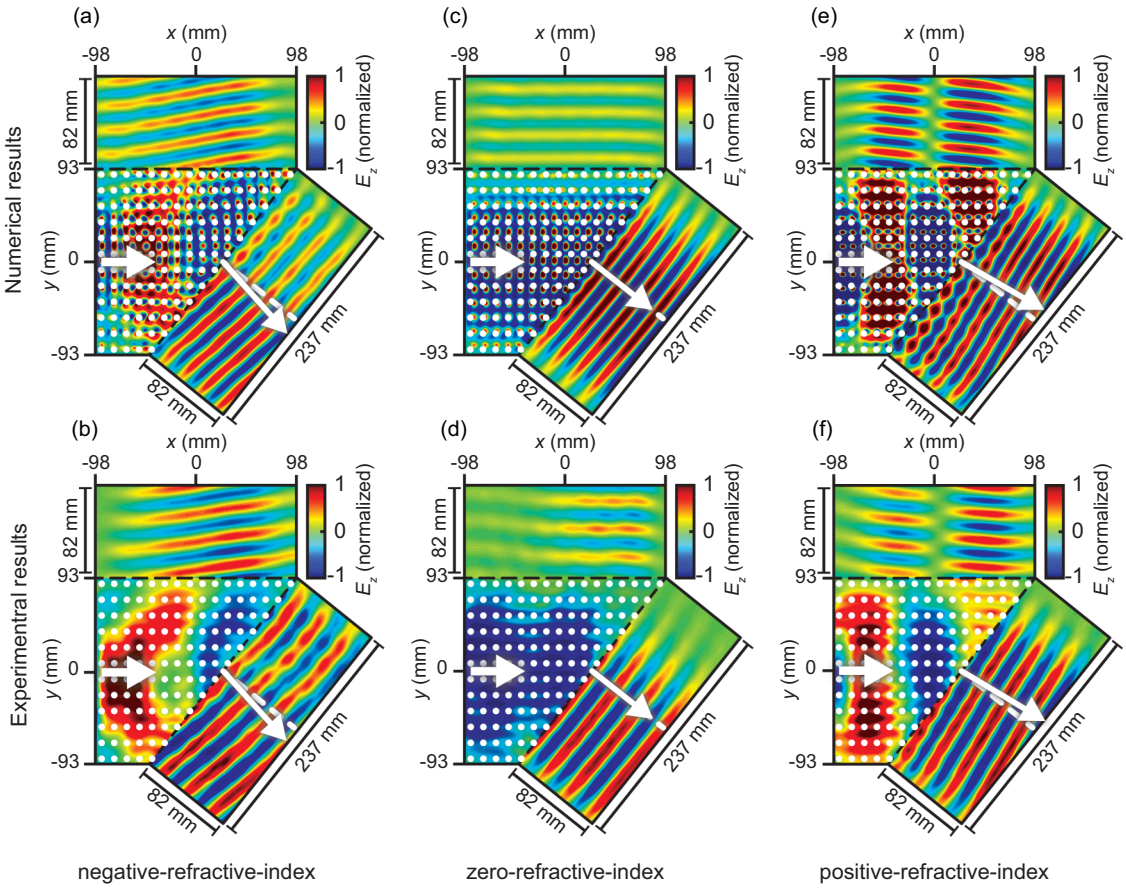

FIG. 7. Simulation and experimental results in the microwave regime to demonstrate semi-Dirac cone dispersion phenomenon. FDTD and experimental results showing real components of the electric field distributions inside and outside of the triangle-shaped PC at frequencies (a, b) below the semi-Dirac point (11.70 GHz), (c, d) at the semi-Dirac point (12.10 GHz), and (e, f) above the semi-Dirac point (12.90 GHz).

in both simulation and experimental results since the semi-Dirac materials have the property of being anisotropic and optically impedance-mismatched along the y direction. At the semi-Dirac frequency, the effective refractive index of alumina PC is calculated as $n_x^{\text{eff}} = -0.003$ along the ΓX symmetry axis using the effective medium parameters given in Fig. 6(b). Besides, the effective refractive index measured from the given electric field profiles is equal to $n_x^{\text{eff}} \approx 0$ (measured) for both simulation and experimental cases. Finally, Figs. 7(e) and 7(f) represent the electric field profiles inside the PCs that show the conventional positive-refraction phenomenon for both simulation and experiment at $f = 12.90$ GHz, respectively. Similarly, both simulation and experimental results are consistent with each other since the phase distributions inside the PCs are alike. In addition, since the effective medium parameters given in Fig. 6(b) are positive ($\varepsilon^{\text{eff}} > 0$, $\mu^{\text{eff}} > 0$) above the semi-Dirac point, exiting beams are refracted positively in both electric field demonstrations. Above the semi-Dirac frequency, the effective refractive index is calculated as $n_x^{\text{eff}} = 0.269$ using the effective medium parameters given in Fig. 6(b). In addition, the measured refractive indices from simulation and experimental results are $n_x^{\text{eff}} \approx 0.251$ (measured, simulation) and $n_x^{\text{eff}} \approx 0.196$ (measured, experiment), respectively. To summarize, the performed FDTD simulations of semi-Dirac materials are verified in the real world via experimental measurements. At the semi-Dirac point, it has been experimentally proven that the periodic structures show a zero-refractive-index phenomenon. Furthermore, the frequencies above and below the semi-Dirac point experimentally exhibited the presence of positive- and negative-refraction-index phenomena, respectively.

IV. CONCLUSION

In this study, we have numerically and experimentally demonstrated that by reducing the order of rotational symmetry of unit cells of PCs exhibiting Dirac-like cone dispersion in the Brillouin zone center, anisotropic zero-refractive-index materials, i.e., periodic media having semi-Dirac dispersion, can be realized. At doubly degenerate frequency, which is the semi-Dirac point, the periodic medium behaves as a double-zero material ($\varepsilon^{\text{eff}} \approx 0$, $\mu^{\text{eff}} \approx 0$) along one propagation direction, whereas it behaves as ENZ material ($\varepsilon^{\text{eff}} \approx 0$, $\mu^{\text{eff}} \neq 0$) for the transverse propagation direction. The PC structures having Dirac-like cone dispersion may require confining materials to design proper photonic devices due to their isotropic dispersion characteristics. In addition, for the selected refractive index of dielectric rods, the Dirac-like frequency is unique, which prevents the designed photonic devices from being configurable. However, semi-Dirac-dispersion-based PCs show anisotropic

behavior and can be easily utilized in photonic applications without the need for any limiting material. In addition, new semi-Dirac points can be generated at different frequencies by only adjusting the aspect ratio of unit cells (or dielectric rods) exhibiting semi-Dirac dispersion. With these advantages, photonic devices such as beam deflectors, beam splitters, and focusing lenses can be realized by exploiting the anisotropic behavior of semi-Dirac materials.

ACKNOWLEDGMENTS

U.G.Y. and H.K. gratefully acknowledge the financial support from the Scientific and Technological Research Council of Turkey (TUBITAK), Project No. 115R036. H.K. also acknowledges partial support of the Turkish Academy of Sciences. The authors also thank the anonymous referee for the illuminating suggestion about a possible connection between the van Cittert–Zernike theorem and zero-refractive-index materials.

[1] E. Yablonovitch, Phys. Rev. Lett. **58**, 2059 (1987).
[2] S. John, Phys. Rev. Lett. **58**, 2486 (1987).
[3] E. Yablonovitch, J. Opt. Soc. Am. B **10**, 283 (1993).
[4] E. Cubukcu, K. Aydin, E. Ozbay, S. Foteinopoulou, and C. M. Soukoulis, Nature (London) **423**, 604 (2003).
[5] J. Witzens, M. Lončar, and A. Scherer, IEEE J. Sel. Top. Quantum Electron. **8**, 1246 (2002).
[6] H. Kosaka, T. Kawashima, A. Tomita, M. Notomi, T. Tamamura, T. Sato, and S. Kawakami, Phys. Rev. B **58**, R10096(R) (1998).
[7] R. A. Sepkhanov, Y. B. Bazaliy, and C. W. J. Beenakker, Phys. Rev. A **75**, 063813 (2007).
[8] M. Diem, T. Koschny, and C. Soukoulis, Physica B: Condensed Matter **405**, 2990 (2010).
[9] S. Raghu and F. D. M. Haldane, Phys. Rev. A **78**, 033834 (2008).
[10] X. Zhang, Phys. Rev. Lett. **100**, 113903 (2008).
[11] X. Huang, Y. Lai, Z. H. Hang, H. Zheng, and C. T. Chan, Nat. Mater. **10**, 582 (2011).
[12] C. T. Chan, X. Huang, F. Liu, and Z. H. Hang, Prog. Electromagn. Res. B **44**, 163 (2012).
[13] P. Moitra, Y. Yang, Z. Anderson, I. I. Kravchenko, D. P. Briggs, and J. Valentine, Nat. Photonics **7**, 791 (2013).
[14] J. W. Dong, M. L. Chang, X. Q. Huang, Z. H. Hang, Z. C. Zhong, W. J. Chen, Z. Y. Huang, and C. T. Chan, Phys. Rev. Lett. **114**, 163901 (2015).
[15] J.-R. Wang, X.-D. Chen, F.-L. Zhao, and J.-W. Dong, Sci. Rep. **6**, 22739 (2016).
[16] C. Xu and Y. Lai, Phys. Rev. B **95**, 045124 (2017).
[17] S. V. Boriskina, Nat. Photonics **9**, 422 (2015).
[18] S. Kita, Y. Li, P. Muñoz, O. Reshef, D. I. Vulis, R. W. Day, E. Mazur, and M. Lončar, Opt. Express **25**, 8326 (2016).
[19] H. Gao, Y. Zhou, and Z. Zheng, J. Opt. **18**, 105102 (2016).
[20] X. T. He, Z. Z. Huang, M. L. Chang, S. Z. Xu, F. L. Zhao, S. Z. Deng, J. C. She, and J. W. Dong, ACS Photonics **3**, 2262 (2016).
[21] S. Enoch, G. Tayeb, P. Sabouroux, N. Guérin, and P. Vincent, Phys. Rev. Lett. **89**, 213902 (2002).
[22] M. Silveirinha and N. Engheta, Phys. Rev. B **75**, 075119 (2007).
[23] A. Alù, M. G. Silveirinha, A. Salandrino, and N. Engheta, Phys. Rev. B **75**, 155410 (2007).
[24] R. Liu, Q. Cheng, T. Hand, J. J. Mock, T. J. Cui, S. A. Cummer, and D. R. Smith, Phys. Rev. Lett. **100**, 023903 (2008).
[25] D. C. Adams, S. Inampudi, T. Ribaudo, D. Slocum, S. Vangala, N. A. Kuhta, W. D. Goodhue, V. A. Podolskiy, and D. Wasserman, Phys. Rev. Lett. **107**, 133901 (2011).
[26] A. Alù, M. G. Silveirinha, and N. Engheta, Phys. Rev. E **78**, 016604 (2008).
[27] M. Silveirinha and N. Engheta, Phys. Rev. Lett. **97**, 157403 (2006).
[28] Y. Wu, Opt. Express **22**, 1906 (2014).
[29] X. T. He, Y. N. Zhong, Y. Zhou, Z. C. Zhong, and J. W. Dong, Sci. Rep. **5**, 13085 (2015).
[30] I. H. Giden and H. Kurt, Appl. Opt. **51**, 1287 (2012).
[31] U. G. Yasa, M. Turduev, I. H. Giden, and H. Kurt, J. Light. Technol. **35**, 1677 (2017).
[32] I. H. Giden, M. Turduev, and H. Kurt, J. Eur. Opt. Soc. **9**, 14045i (2014).
[33] M. Hammermesh, *Group Theory and Its Application to Physical Problems* (Dover, New York, 1962).
[34] M. Glazer and G. Burns, *Space Groups for Solid State Scientists* (Academic Press, New York, 2013).
[35] S. Johnson and J. Joannopoulos, Opt. Express **8**, 173 (2001).
[36] K. Busch and S. John, Phys. Rev. Lett. **83**, 967 (1999).
[37] H. T. Chen, W. J. Padilla, J. M. O. Zide, A. C. Gossard, A. J. Taylor, and R. D. Averitt, Nature (London) **444**, 597 (2006).
[38] Y. Y. Wang and L. W. Chen, Opt. Express **14**, 10580 (2006).
[39] H. Rauh, G. I. Yampolskaya, and S. V. Yampolskii, New J. Phys. **12**, 073033 (2010).
[40] W. M. Zhu, A. Q. Liu, T. Bourouina, D. P. Tsai, J. H. Teng, X. H. Zhang, G. Q. Lo, D. L. Kwong, and N. I. Zheludev, Nat. Commun. **3**, 1274 (2012).
[41] C. H. Ho, Y. C. Cheng, L. Maigyte, H. Zeng, J. Trull, C. Cojocaru, D. S. Wiersma, and K. Staliunas, Appl. Phys. Lett. **106**, 021113 (2015).
[42] H. Kurt, M. Turduev, and I. H. Giden, Opt. Express **20**, 7184 (2012).
[43] Lumerical Inc., http://www.lumerical.com/tcad-products/fdtd/
[44] M. Born and E. Wolf, *Principles of Optics: Electromagnetic Theory of Propagation, Interference and Diffraction of Light* (Pergamon, Exeter, U.K., 1994).
[45] Y. Lai, Y. Wu, P. Sheng, and Z. Q. Zhang, Nat. Mater. **10**, 620 (2011).
[46] Z. Cui, *Nanofabrication: Principles, Capabilities and Limits* (Springer, Berlin, 2017).